Postprint of: Kiwilszo M., Zieliński A., Smulko J., Darowicki K., Improving AFM Images with Harmonic Interference by Spectral Analysis, Microscopy and Microanalysis, Vol. 18, Iss. 1 (2012), pp. 186–195, DOI: 10.1017/S1431927611012281

IMPROVING AFM IMAGES WITH HARMONIC INTERFERENCE BY SPECTRAL ANALYSIS

Marek Kiwilszo[1], Artur Zieliński[2], Janusz Smulko[1], Kazimierz Darowicki[2]

[1]Faculty of Electronics, Telecommunications and Informatics, Department of Optoelectronics and Electronics Systems, Gdańsk University of Technology, Narutowicza Str. 11/12, 80-233 Gdańsk, POLAND

[2]Chemical Faculty, Department of Electrochemistry, Corrosion and Material Engineering, Gdańsk University of Technology, Narutowicza Str. 11/12, 80-233 Gdańsk, POLAND

Gdańsk, Poland, Marek.Kiwilszo@gmail.com

Abstract

Atomic force microscopy (AFM) is one of the most sensitive tools for nanoscale imaging. As such, it is very sensitive to external noise sources that can affect the quality of collected data. The intensity of the disturbance depends on the noise source and the mode of operation. In some cases, the internal noise from commercial AFM controllers can be significant and difficult to remove. Thus, a new method based on spectrum analysis of the scanned images is proposed to reduce harmonic disturbances. The proposal is a post-processing method and can be applied at any time after measurements.

This paper encloses a few methods of harmonic cancellation (e.g. median filtering, wavelet denoising, Savitzky-Golay smoothing) and compares their effectiveness. The proposed method, based on Fourier transform of the scanned images, was more productive than the other methods mentioned before. The presented data were achieved for images of conductive layers taken in a contact AFM mode.

Introduction

Scanning probe microscopy has been developed since the eighties of the twentieth century. In 1979, G. Binnig and H. Rohrer presented the first patent application concerning the scanning tunneling microscope (STM). The prototype device was built in 1982. A deeper look into STM microscopy gave rise to the development of an atomic force microscope — AFM (Binnig et al., 1986). A better versatility, when compared to STM, assured its wide use in life sciences (Stark et al., 2003, Langer et al., 2000, Marsh et al., 1995), material engineering (Lee et al., 2010, Saha, 2010, Göken & Vehoff, 1996) and physics (Mohideen & Roy, 1998). The measurements of friction forces, roughness, hardness and Young modulus on a molecular level can be performed. Another important advantage of this technique is its use in various surroundings (vacuum, liquid), which is crucial for biology as well as for electrochemistry.

The use of AFM in different working modes and conditions is often disturbed by noise sources (e.g. harmonic interferences) that cannot be reduced during measurements. The distortions were observed many times and different methods were introduced to limit their intensity (Eaton & West, 2010, Mendez-Vilas et al., 2002, West & Starostina, Westra et al., 1993). However, we still need to improve or automate these methods to enhance their efficiency.

Troublesome electrical interference is present at measurements when an oscillating signal is introduced to the cantilever or sample. A good example is nanoimpedance imaging. This method measures the current flowing between the probe polarized by a harmonic voltage and the investigated sample. The current is observed during surface scanning at the selected rate of the probe movement. The modulus of the measured current gives information about the impedance of the scanned surface at a given location and at the frequency of the applied polarizing voltage. Such information is very useful for the evaluation of paintings and anticorrosive coatings and can be presented as an image of the scanned surface. A more detailed description of this methodology can be found in numerous references (O'Hayre et al., 2004, Ciureanu & Wang, 2000, Fleig, 2002, Popkirov & Barsoukov, 1995, Shim et al., 1990).

The measured current is disturbed by harmonic components, that should be attenuated to improve the quality of the collected images. Unfortunately, any hardware improvements are excluded due to the limited access and quality of the microscope controller. Therefore, a new software method was proposed and the results were compared with other algorithms, that could be used as well but are less efficient.

Image acquisition process

Three samples were scanned using the NTEGRA Prima device, each using an AFM topography scan and surface impedance scan (Fig. 1). Sample 1 was a gold plate used as a reference. Sample 2 was an example of a typical scanned paint coating. Sample 3 was a pre-pressed compact disc (CD-ROM) covered with a conductive layer and with a visible pattern of bytes. Table 1 summarizes the parameters of the scanning process for the investigated samples. The selected samples were conductive, which allowed for the contact AFM mode nanoimpedance measurements. The gold sample was very even and, therefore, all harmonic interferences were easily identified by visual inspection of the analyzed images. The sample of an epoxy coating was an example of the practical application of the nanoimpedance measurement technique used to characterize anticorrosion coatings. The last selected sample of CD-ROM was used to present a regular image of a well-known structure in the AFM technique.

A sinusoidal voltage with a constant amplitude and frequency was used as the excitation signal during the nanoimpedance scanning. As a response, the current between the probe and the sample was measured. Since the voltage parameters were constant during scanning, the current depended on the impedance of the samples and, therefore, gave information that could characterize the quality of the investigated coating. The measurements were limited to single-frequency scans with simultaneous scanning of the surface. The tip moved along the space coordinate with an assumed linear speed. Movement commenced discretely with the assumed sampling time for each pixel. In such case, during a given time period, the direct proximity of the surface point is perturbed by a selected potential signal. This signal together with the current response signal determines the value of impedance around the surface point.

In the reported configuration, the generation of the perturbation signal and spectral analysis were performed by built-in circuitry of the AFM device producing an image of the alternating current modulus distribution over the surface. The measured current exhibited interference of a few harmonic components due to limitations of commercial AFM controllers. These components limited the accuracy of AFM image analysis and should be removed. The images were recorded in the ambient atmosphere of laboratory air at room temperature.

Amplitudes of the measured currents were exported into a text file and saved as a 2D matrix of floating numbers. The AFM scanned image of the relative height was saved to a text

file as a 2D matrix in the same way. The results were imported into Matlab software and visualized as independent images of relative height (Fig. 2) or module of the measured current (Fig. 3). The input values were linearly mapped into a grey-scale color map of 256 levels, which is commonly used for visual analysis. The minimum value is displayed as black and the maximum value as white. All values between are displayed as grey shades.

Methods of interference removals

The harmonic artifacts present during the measurements are shown in Fig. 3. A visible mesh interference is clearly exposed and decreases the usefulness of the images acquired for further detailed analysis. Thus, the main aim of the presented paper is to attenuate those disturbances. The analysis was performed using Matlab software, image processing and Wavelet toolboxes and was focused on proposing a method that could be performed automatically without operator knowledge. The following attempts were performed to select the method that was most effective. All the attempts are presented to show the differences in the achieved results.

Median filtering

Since the observed disturbances have a few high-frequency components, the denoising procedure was applied. First, a 2D median filter was performed by using the *medfilt2* function. Median filtering is a nonlinear operation often used in image processing to reduce the *salt-and-pepper* noise. This filter is more effective than a convolution operation when we want to reduce noise and preserve edges at the same time (Koay et al., 2002).

Wavelet denoising

Another alternative denoising method uses the wavelet transform. A few different wavelets (e.g. *db*, *sym*, *coif*, *bior*) were tested with various parameters and at different decomposition levels using hard and soft thresholding. The wavelet denoising procedure was implemented using the *wdencmp* function of the Wavelet toolbox in Matlab.

Spectral dumping of the selected harmonics

A visual inspection of impedance scans confirms that disturbances do not depend on the topography of the scanned surface. Furthermore, such disturbances are periodic. It is reasonable to consider the observed interferences as an additive periodic function, which is

the sum of a few harmonic components. Thus, the next trial was focused on disturbance identification and their most effective removal.

Calculating the spectrum for each row and averaging the amplitude of all row-spectra by the number of rows gives an average row-spectrum amplitude of the acquired image. Doing the same for columns gives an average column spectrum amplitude.

Let us describe an image as an $M \times N$ matrix $a\,(x, y)$ of the grey-scale values:

$$\begin{bmatrix} a_{(1,1)} & \dots & a_{(x,1)} & \dots & a_{(M,1)} \\ a_{(1,y)} & \dots & a_{(x,y)} & \dots & a_{(M,y)} \\ a_{(1,N)} & \dots & a_{(x,N)} & \dots & a_{(M,N)} \end{bmatrix}. \tag{1}$$

The spectrum of the selected y-row can be described as:

$$A_{r,y}(k) = \sum_{x=1}^{M} a_{x,y} \cdot e^{-j\frac{2\pi}{M}k \cdot x} \quad \text{for } k = 0, \dots, M-1. \tag{2}$$

The average module of the row spectrum is given as:

$$\left|A_r(k)\right| = \frac{1}{N}\sum_{y=1}^{N}\left|A_{r,y}(k)\right| = \frac{1}{N}\sum_{y=1}^{N}\left|\sum_{x=1}^{M} a_{x,y} \cdot e^{-j\frac{2\pi}{M}k \cdot x}\right| \quad \text{for } k = 0, \dots, M-1. \tag{3}$$

Doing the same for columns, we can define the average column-spectrum amplitude:

$$\left|A_c(k)\right| = \frac{1}{M}\sum_{x=1}^{M}\left|A_{c,x}(k)\right| = \frac{1}{M}\sum_{x=1}^{M}\left|\sum_{y=1}^{N} a_{x,y} \cdot e^{-j\frac{2\pi}{N}k \cdot y}\right| \quad \text{for } k = 0, \dots, N-1. \tag{4}$$

Assuming that the disturbance from the scanned line to line is the same, the average spectrum of the row/column should reveal the type of observed disturbance. The averaged spectrum of images of the scanned current module contains visible peaks, that are not present in images of the AFM relative height scans. We can suspect that these peaks are responsible for the mesh present on the acquired images. To confirm this assumption and to minimize influence of the sample undisturbed image on the estimated spectra, the analysis was done for the homogeneous sample of a gold plate. That sample is conductive and images of relative high and of current modules with sinusoidal voltage excitation can be measured as well.

Figure 4 shows differences between the AFM relative height scan and the current module scan of the same gold plate called sample 1. The disturbing mesh is clearly visible in the scan when the sinusoidal excitation signal was used (Fig. 4, right), while it is not identified during the AFM relative height scan (Fig. 4, left). Figure 5 and Figure 6 compare

the averaged spectra of images obtained for both types of scans (Fig. 4) using formulas (3) and (4) for rows and columns, separately. The averaged spectrum of the current module image (Fig. 6) reveals peaks that are not present in the averaged spectrum of the AFM relative height image (Fig. 5). We can assume that the observed peaks identify the disturbing harmonic components. The same analysis was done for the epoxy protective coating (sample 2) that shows a more diverse image (Fig. 7) than the previously analyzed gold plate. Even a general inspection of the peaks shows that some of them can be grouped into similar harmonics sets.

The recognized interference suggested the following algorithm, that is based on Fourier transform, and comprises:

- calculation of the averaged spectrum for rows and columns;
- identification of frequencies of the suspected harmonic interferences;
- Fourier transform of each image row into the frequency domain;
- removal of the identified peaks in each amplitude spectrum of the image row by replacing by averaged adjacent values;
- inverse Fourier transform of image row from the frequency domain to the image space domain;
- Fourier transform of each image column into the frequency domain;
- removal of the identified peaks in each amplitude spectrum of the image column by replacing them with averaged adjacent values,
- inverse Fourier transformation of the image row from the frequency domain to the image space domain.

The presented algorithm was modified by replacing the signal phase at the identified interference frequencies in the row and column spectra with a random value uniformly distributed within the range $0 \div 2\pi$. No significant change was observed in the achieved images. Thus, the proposed algorithm was restricted only to the amplitude spectrum.

Fourier transforms between space and frequency domains for each row and column were performed using the Matlab functions, *fft* and *ifft*. The selected peaks were attenuated by applying formulas of the arithmetical averaging for rows and columns separately:

$$A_{r,k-P}(y) : A_{r,k+P}(y) = \frac{1}{2}\left(A_{r,k-P-1}(y) + A_{r,k+P+1}(y)\right), \tag{5}$$

$$A_{c,k-P}(y) : A_{c,k+P}(y) = \frac{1}{2}\left(A_{c,k-P-1}(y) + A_{c,k+P+1}(y)\right), \tag{6}$$

where k is the frequency at which the peak was identified. The number of the frequency bins used for being attenuated was selected experimentally to nine ($P = 4$) for sample 1 and

sample 2 due to the adjusted image resolution and width of the observed peaks. For the sample 3 (CD-ROM image), the attenuation was limited only to three adjacent frequency bins ($P = 1$).

The peaks, that were attenuated in the analyzed spectra, were selected manually by choosing the peaks with amplitudes twice bigger than the background level estimated by the average value of a few adjacent frequency bins. The peak selection can be performed automatically by calculating the derivative of the analyzed spectra and comparing its module with the assumed threshold level.

The mesh-type interference was observed sometimes in the vertical or horizontal direction only. That fact corresponded to the presence of interference peaks in the averaged spectra of rows or of columns only. In such cases, the proposed algorithm could be limited to rows or columns only where the disturbing mesh had dominant components. Such an approach would limit computations and possible distortions caused by unnecessary image modifications during the application of the proposed algorithm.

Savitzky-Golay smoothing

The above-mentioned remark about images exhibiting disturbances only in one direction leads to another proposal of a denoising method. A Savitzky-Golay low-pass filter can be used to smooth such data and reduce high-frequency harmonic interferences (Press et al., 2007). That filter can be applied by using the function, *sgolayfilt*, that is available in the Matlab software. The function treats each row (column) of the analyzed image as an elementary vector containing original data and unwanted interference. The analyzed image is processed row by row (or column by column) depending on the direction, where the major interference is observed. That method requires the choice of a polynomial order for the low-frequency component identification, that is a compromise between preventing image details and noise reduction. Apart from the statistical methods described in literature for the optimal Savitzky-Golay filter parameter selection (Thornley, 2006, Wilson, 2006), we tuned in the filter parameters (order and length of the window) experimentally to get the most satisfying results. After an incremental tryout, the following parameters were selected:

- for the sample 1: polynomial order = 5; window length = 11;
- for the sample 2: polynomial order = 5; window length = 25.

Results and discussion

All the analyzed images of AFM nanospectroscopy had visible interferences and there was no image that could be used as a model. Therefore, it was possible to compare only images obtained after applying various algorithms of interference reduction to establish the efficiency of the applied methods. An improvement of the analyzed image is usually estimated by the intensity of the remaining noise component, e.g. Mean Square Error (MSE) or Peak-Signal-to-Noise Ratio (PSNR). These methods assume that the noise component is the Additive White Gaussian Noise (AWGN) (Liu et al., 2007, Dengwen, 2007, Protter & Elad, 2009). In our case, the observed interference is the sum of a few harmonics, which are strongly localized frequency components. This is in contrast with white noise, that is evenly distributed within all frequencies. Therefore, the quality of the resulting images should be estimated by visual review only.

The applied median denoising was not effective in removal of the harmonic interferences. A noticeable effect was blurring with a short filter window, without any visible reduction of the existing distortions. When the size of the applied filter window exceeded 9x9 pixels, the interferences were evidently smoothed but with accompanying serious drop of image quality. These results are shown in Fig. 8 for a small filter window (3x3 pixels) and in Fig. 9 for the greater window (9x9 pixels).

The efficiency of a denoising algorithm based on wavelet transform depended strongly on the value of the selected threshold. Some improvements were noticed for soft thresholding. Image quality was slightly better than previously noticed for median filtering. However, the interferences were still clearly visible. Figure 10 shows the results of denoising obtained for the wavelet function *db4* and manually tuned threshold levels.

A limited reduction of interferences using median filtering or wavelet denoising results from a type of disturbance, that comprises a few main frequency components. The applied algorithms are more efficient for noise removal than for harmonic components. The method proposed by the authors gave much better results. Figure 11 compares the recorded image of sample 1 with the clear mesh-type interferences and its improved version by applying a Fourier-transform-based algorithm. Figure 12 presents the result obtained for the same algorithm for the image of sample 2. The mesh diminished strongly its presence, together with preserving the object edges. Unfortunately, the proposed algorithm did not remove the noise component, that was still visible (Fig. 12). That disadvantage can be easily

improved by applying one of two other algorithms (wavelet denoising or Savitzky-Golay filtering).

The Fourier-transform-based algorithm can be restricted to rows or columns of the analyzed image only when a dominant disturbance component is exclusively vertical or horizontal. Such a limitation, that resulted in less intensive computations, should also give reasonable results, but due to signal windowing and spectra leakage, the best results were obtained when the algorithm was applied to rows and columns as well. The narrow vertical stripes on the left and right sides of the image with visible interferences were observed when the algorithm was applied to rows only (fast scan direction).

When the analyzed image comprises a repeatable pattern, like in the case of CD-ROM (Fig. 13), the proposed algorithm has to be applied more carefully. Some of frequency spikes present in the averaged spectra of columns or rows are generated by the observed pattern and have to be identified before applying the proposed algorithm. Otherwise, the main image pattern will be deformed. The presented image of the CD-ROM (sample 3) comprises a pattern of oval series with a visible mesh-type interference on background, that was emphasized by applying a non-linear grey scale (Fig. 14). The averaged spectra of image columns or rows exhibit a few frequency peaks generated by the pattern of oval series at a low-frequency range (Fig. 15). The harmonic interferences are located in the higher frequency range. When the proposed algorithm is applied to the mentioned high frequency range only (for $k > 25$), we can reduce its presence as well, but effectiveness is worse than for sample 1 and sample 2 without such repeatable patterns (Fig. 15).

Conclusions

The scans of AFM nanoimpedance images of the examined samples were investigated to establish an effective algorithm of the observed mesh-type interference removal. The distortions observed were identified as the sum of a few harmonics. Different algorithms were proposed and used to attenuate their presence. The most effective algorithm, which was proposed by the authors, applies the Fourier transform and removes the identified spikes from the spectra of the consecutive columns and rows of the analyzed image by averaging a few adjacent bins.

Other considered methods were much less effective or led to some image blurring. The presented method can be easily enhanced by automatic frequency identification of the interfering harmonics within an averaged row or column spectrum before their removal. Other methods are much less prone to their automatic use.

References

BARSUKOV, E., & MACDONALD, J.R. (2005). *Impedance Spectroscopy*. Hoboken: John Wiley & Sons Inc.

BINNIG, G., QUATE, C.F. & GERBER, CH. (1986). Atomic Force Microscope. *Phys. Rev. Lett.* **56**, 930-933.

BINNIG, G. & ROHRER, H. (1987). Scanning tunneling microscopy - from birth to adolescence. *Rev. Mod. Phys.* **59**, 615-625.

BYKOV, V.A. (2004). New developments in NT-MDT microscope line, pp. 73-74. Nizhni Novgorod: SPM-2004 Proceedings.

CIUREANU, M. & WANG, H. (2000). Electrochemical impedance study of anode CO-poisoning in PEM fuel cells. *J. New Mat. Electrochem. Systems* **3**, 107-119.

DENGWEN, Z. (2007). An Image Denoising Algorithm with an Adaptive Window; pp. I-336-I-336. IEEE International Conference on Image Processing.

EATON, P., WEST, P. (2010) AFM image artifacts. *Atomic Force Microscopy* **19**, 121-139.

FLEIG, J. (2002). The grain boundary impedance of random microstructures: numerical simulations and implications for the analysis of experimental data. *Solid State Ionics* **150**, 181-193.

GIESSIBL, F.J. (2003). Advances in atomic force microscopy. *Rev. Mod. Phys.* **75**, 949-983.

GÖKEN, M. & VEHOFF, H. (1996). Quantitative Metallography of Structural Materials with the Atomic Force Microscope. *Scripta Mater* **35**, 983-989.

KOAY, S.Y., RAMLI, A.R., LEW, Y.P., PRAKASH, V. & ALI, R. (2002). A motion region estimation technique for web camera applications, pp. 352-355. SCOReD Student Conference on Research and Development.

LANGER, M.G., KOITSCHEV, A., HAASE, H., REXHAUSEN, U., HORBER, J.K. & RUPPERSBERG, J. P. (2000). Mechanical stimulation of individual stereocilia of living cochlear hair cells by atomic force microscopy. *Ultramicroscopy* **82**, 269-278.

LEE, G., JUNG, H., SON, J., NAM, K., KWON, T., LIM, G., HO KIM, Y., SEO, J., WOO LEE, S. & SUNG YOON, D. (2010). Experimental and numerical study of electrochemical nanomachining using an AFM cantilever tip. *Nanotechnology* **21**, 185301.

LIU, C., SZELISKI, R., KANG, S.B., ZITNICK C.L. & FREEMAN, W.T. (2008). Automatic estimation and removal of noise from a single image. *IEEE T Pattern Anal.* **30**, 299-314.

MARSH, T.C., VESENKA, J. & HENDERSON, E. (1995). A new DNA nanostructure, the G-wire, imaged by scanning probe microscopy. *Nucleic Acids Res.* **23**, 696-700.

MÉNDEZ-VILAS, A., GONZÁLEZ-MARTÍN, M. L. & NUEVO, M. J. (2002). Optical interference artifacts in contact atomic force microscopy images. *Ultramicroscopy* **92**, 243-250.

MOHIDEEN, U. & ROY, A. (1998). Precision measurement of the Casimir force from 0.1 to 0.9 μm. *Phys. Rev. Lett.* **81**, 4549-4552.

O'HAYRE, R., LEE, M., PRINZ, F.B. (2004). Ionic and Electronic Impedance Imaging Using Atomic Force Microscopy. *J. App. Phys.* **95**, 8382-8392.

POPKIROV, G.S. & BARSOUKOV, E. (1995). In-situ impedance spectra investigation during oxidation and reduction of conductive polymers. Significance of the capacitive currents. *J. Electroanal. Chem.* **383**, 155-160.

PRESS, W.H., TEUKOLSKY, S.A., VETTERLING, W.T. & FLANNERY, B.P. (2007). *Numerical Recipes - The Art of Scientific Computing*. Cambridge, New York: Cambridge University Press.

PROTTER, M., & ELAD, M. (2009). Image sequence denoising via sparse and redundant representations. *IEEE T Image Process* **18**, 29-35.

SAHA, B., LIU, E., TOR, S.B., KHUN, N.W., HARDT, D.E., & CHUN, J.H. (2010). Replication performance of Si-N-DLC-coated Si micro-molds in micro-hot-embossing. *J Micromech Microeng* **20**, 045007.

SHIM, Y.B., WON, M.S. & PARK, S.M. (1990). In-situ spectroelectrochemical studies of polyaniline growth mechanisms. *J Electrochem Soc* **137**, 538-544.

STARK, R.W., RUBIO-SIERRA, F.J., THALHAMMER, S. & HECKL, W.M. (2003). Combining mechanical manipulation by atomic force microscopy with UV-laser micro beam manipulation. *Eur Biophys J* **32**, 33-39.

THORNLEY, D.J. (2006). *Anisotropic Multidimensional Savitzky-Golay Kernels for Smoothing, Differentiation and Reconstruction*. London: Imperial College London Technical Note.

WEST P., STAROSTINA N., *A Guide to AFM image artifacts*. Pacific Nanotechnology, Inc. Technical Note.

WESTRA, K. L., MITCHELL, A. W., THOMSON, D. J. (1993) Tip artifacts in atomic force microscope imaging of thin film surfaces. *J. of Applied Physics* **74**, 3608-3610.

WILSON, D.I. (2006). The black art of smoothing, *Electrical & Automation Technology*, **(June/July)**, 35-36.

Figure and table captions

Fig. 1. Measurement setup.

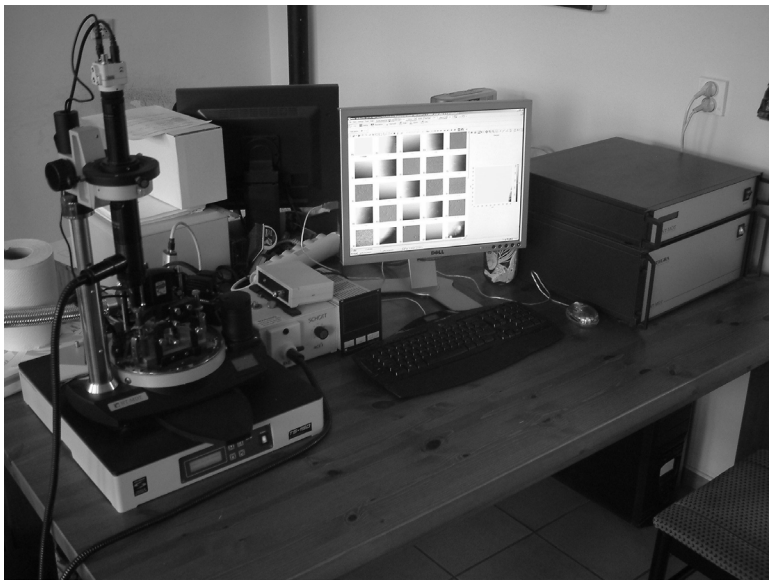

Fig. 2. The AFM image of the relative height of an epoxy protective coating (sample 2).

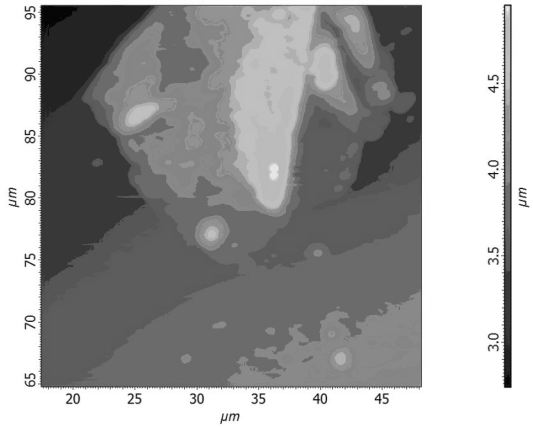

Fig. 3. The AFM image of the module of current flowing between the probe and the sample in the scanned sample 2 with a visible mesh type interference.

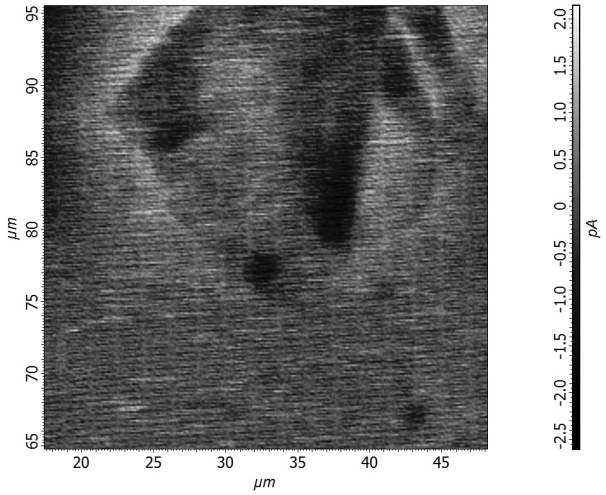

Fig. 4. The AFM image of the relative height (left) and the image of the module of current (right) flowing between the probe and the sample of gold plate (sample 1).

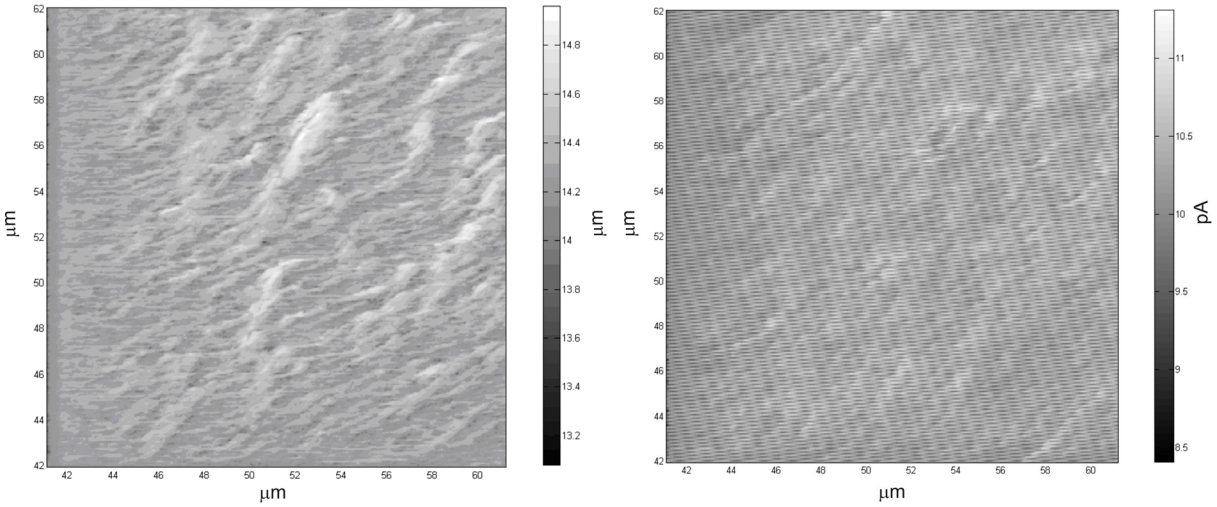

Fig. 5. The averaged spectrum of the AFM relative height scan of the gold plate (sample 1).

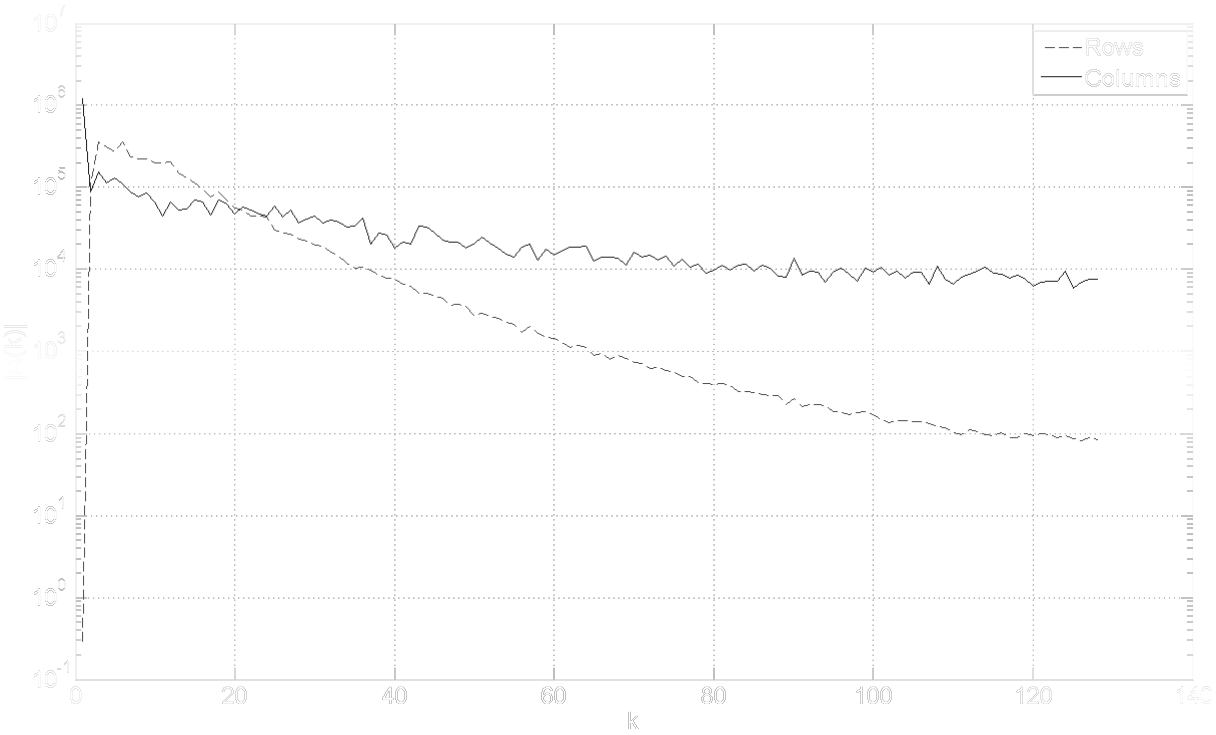

Fig. 6. The averaged spectrum of the AFM scan of the module of current measured with an excitation sinusoidal voltage signal of the gold plate (sample 1).

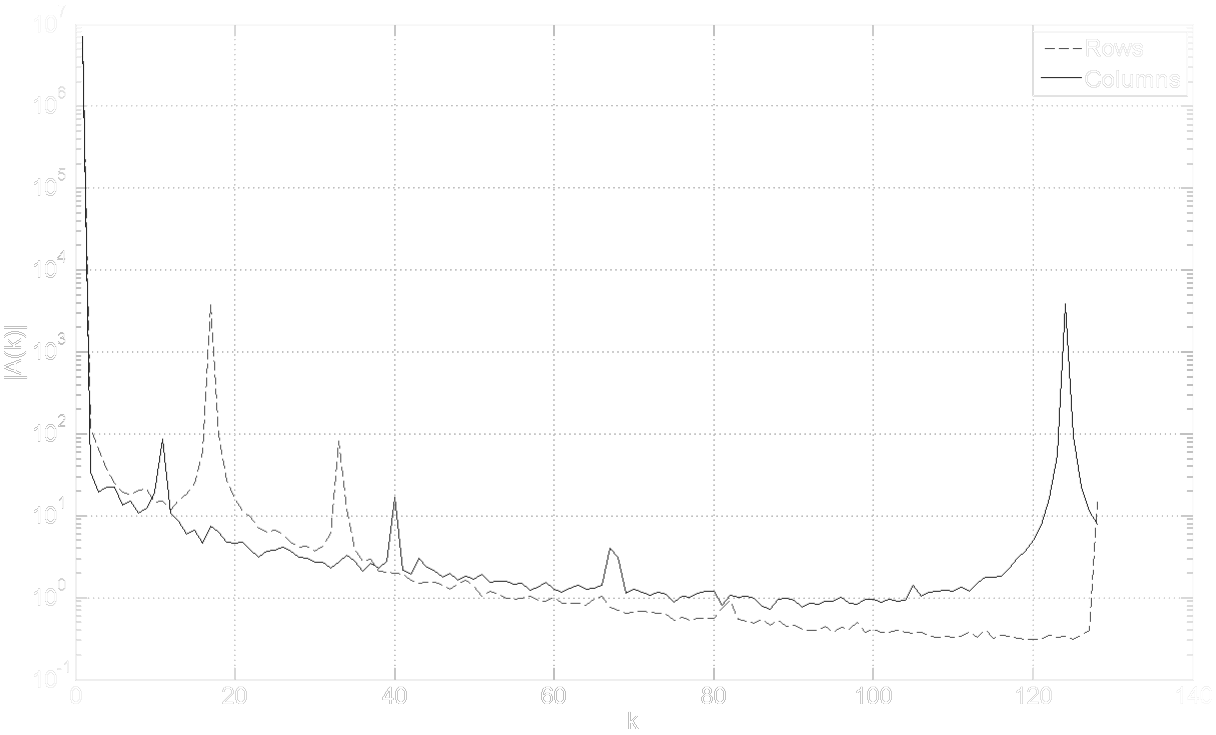

Fig. 7. The averaged spectrum of the AFM scan of the module of current measured with an excitation sinusoidal voltage signal of an epoxy protective coating (sample 2).

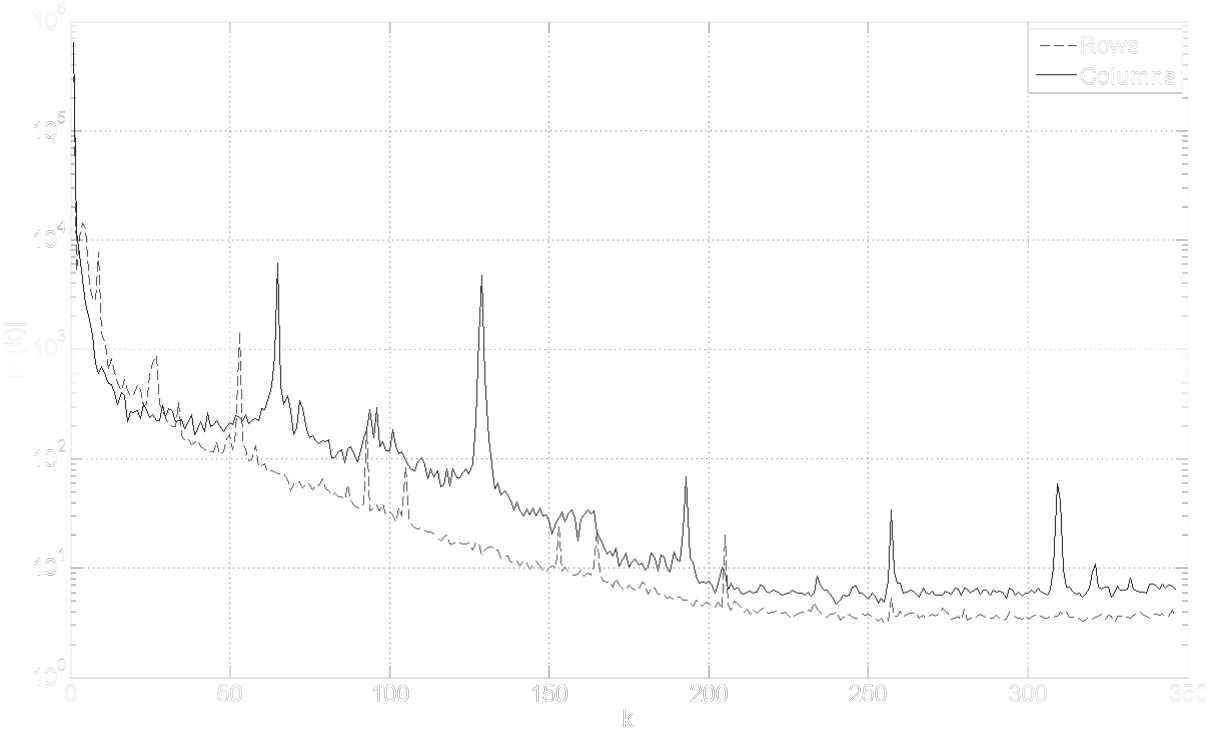

Fig. 8. The AFM nanoimpedance image of sample 2 (left) and after using a median filter (right) with a filtering window of 3x3 pixel size.

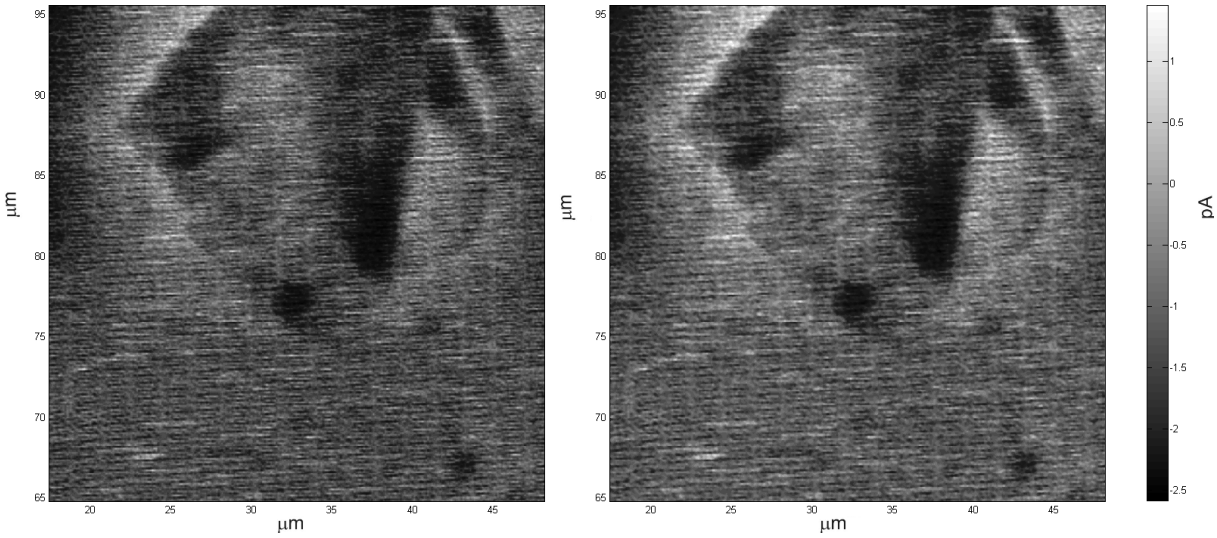

Fig. 9. The AFM nanoimpedance image of sample 2 (left) and after using a median filter (right) with a filtering window of 9x9 pixel size.

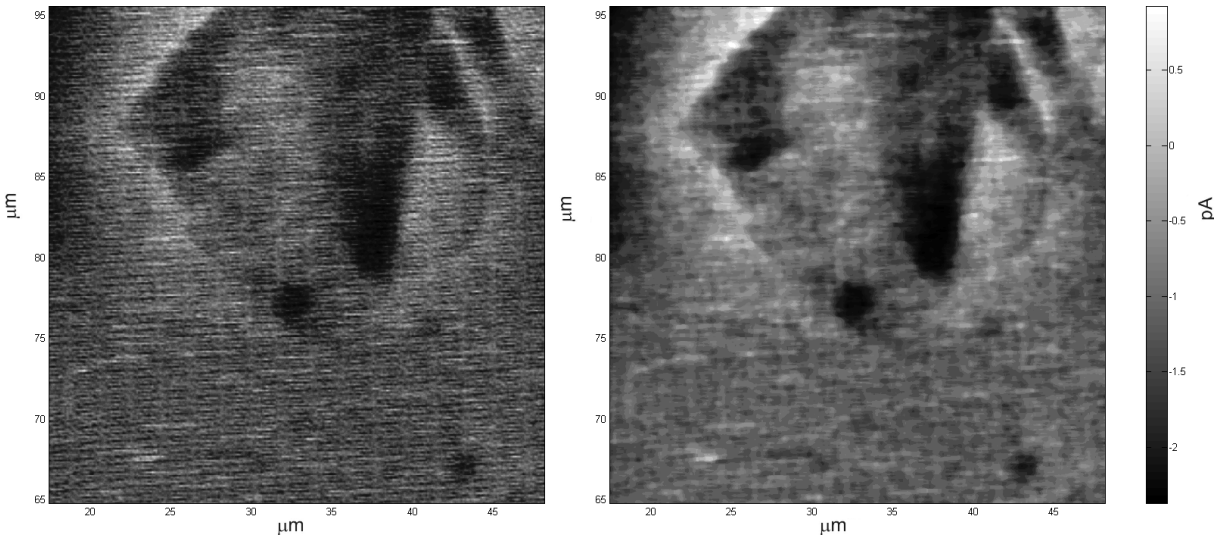

Fig. 10. The AFM nanoimpedance image of sample 2 (left) and after applying wavelet denoising (right) using wavelet function db4 and manually tuned threshold levels.

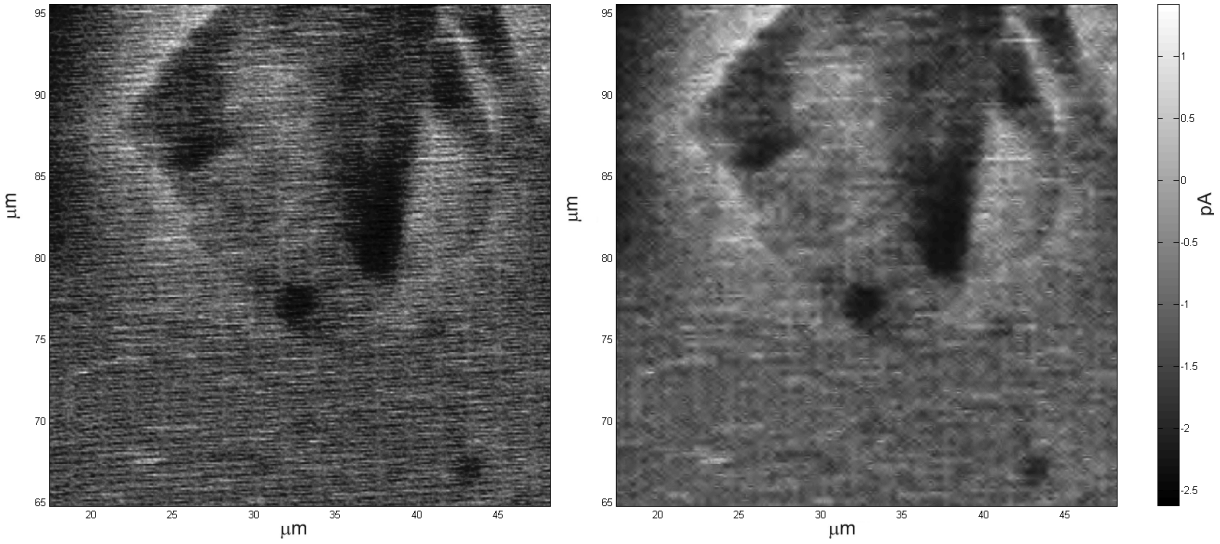

Fig. 11. The AFM nanoimpedance image of sample 1 (left) and after applying the algorithm proposed by the authors (right).

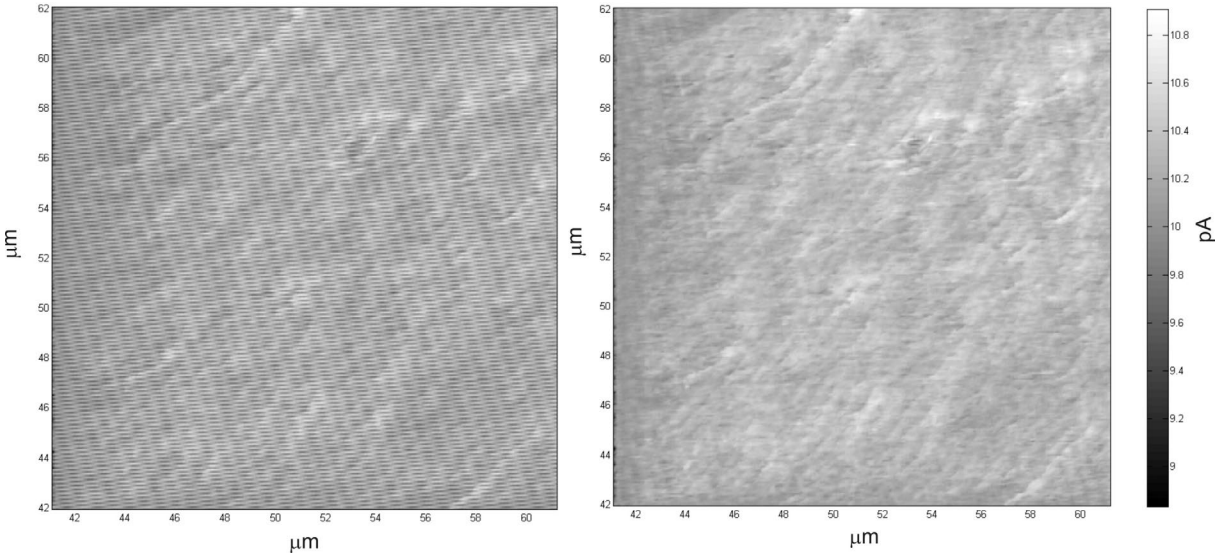

Fig. 12. The AFM nanoimpedance image of sample 2 (left) and after applying the algorithm proposed by the authors (right).

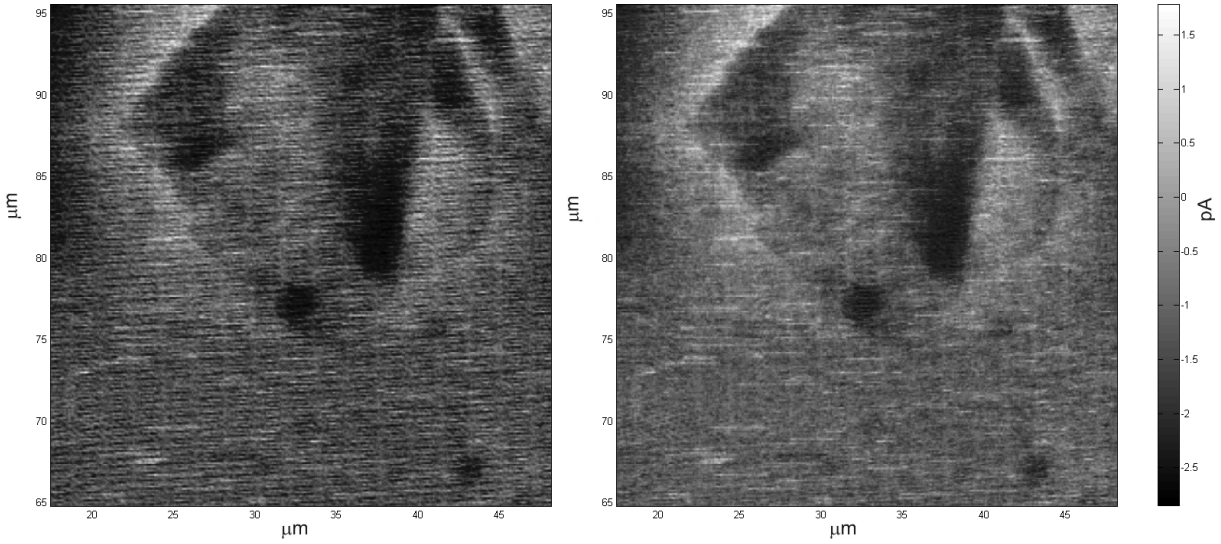

Fig. 13. The AFM image of the relative height of a CD-ROM covered with a conductive layer (sample 3).

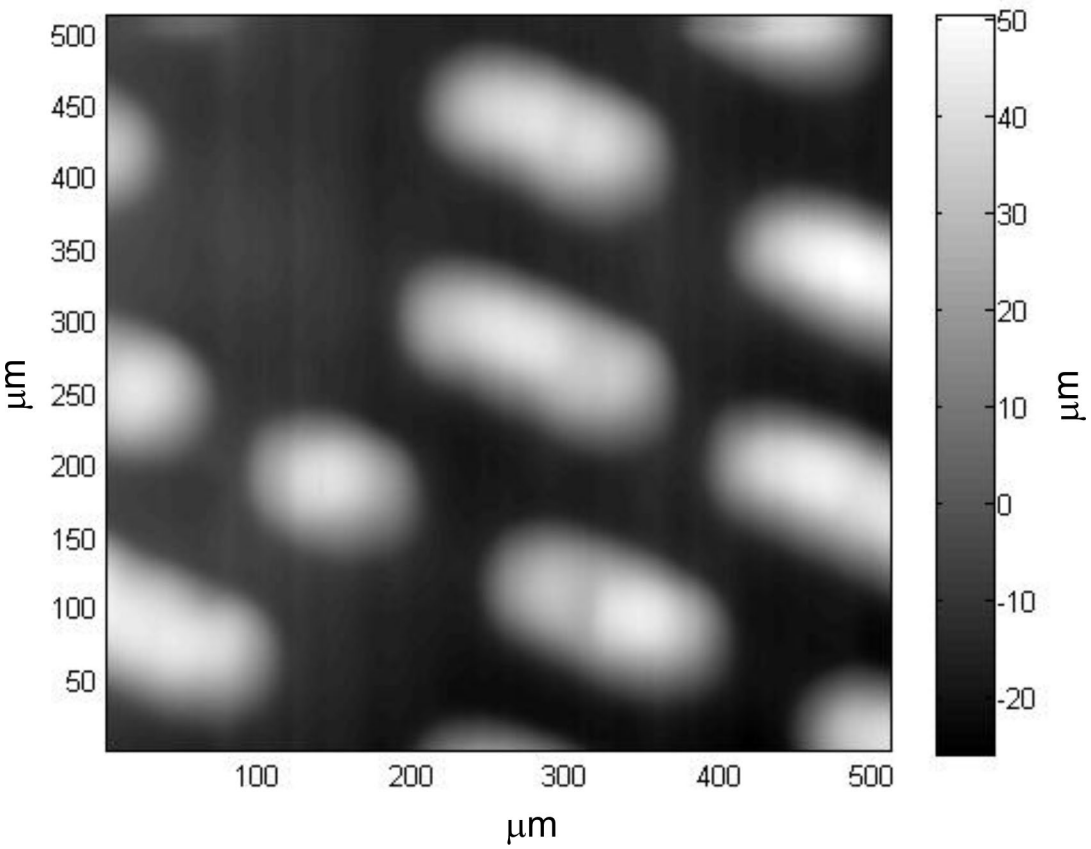

Fig. 14. The AFM nanoimpedance image of sample 3 (left) and after applying the algorithm proposed by the authors (right) using nonlinear gray scale.

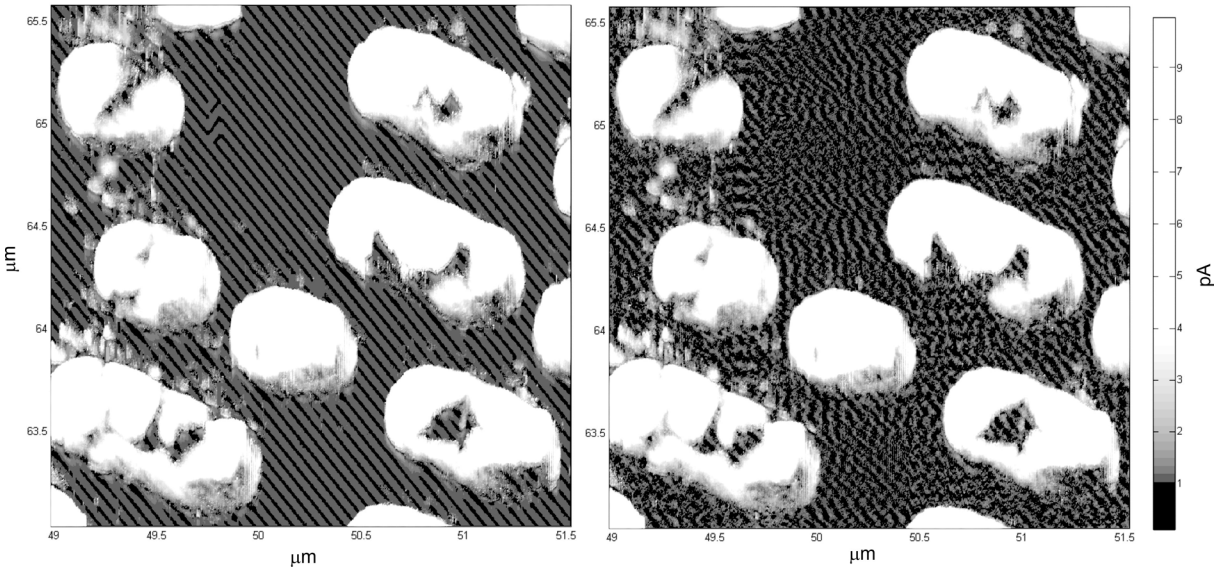

Fig. 15. Averaged spectrum of the AFM scan of the module of current measured with an excitation sinusoidal voltage signal of a CD-ROM (sample 3).

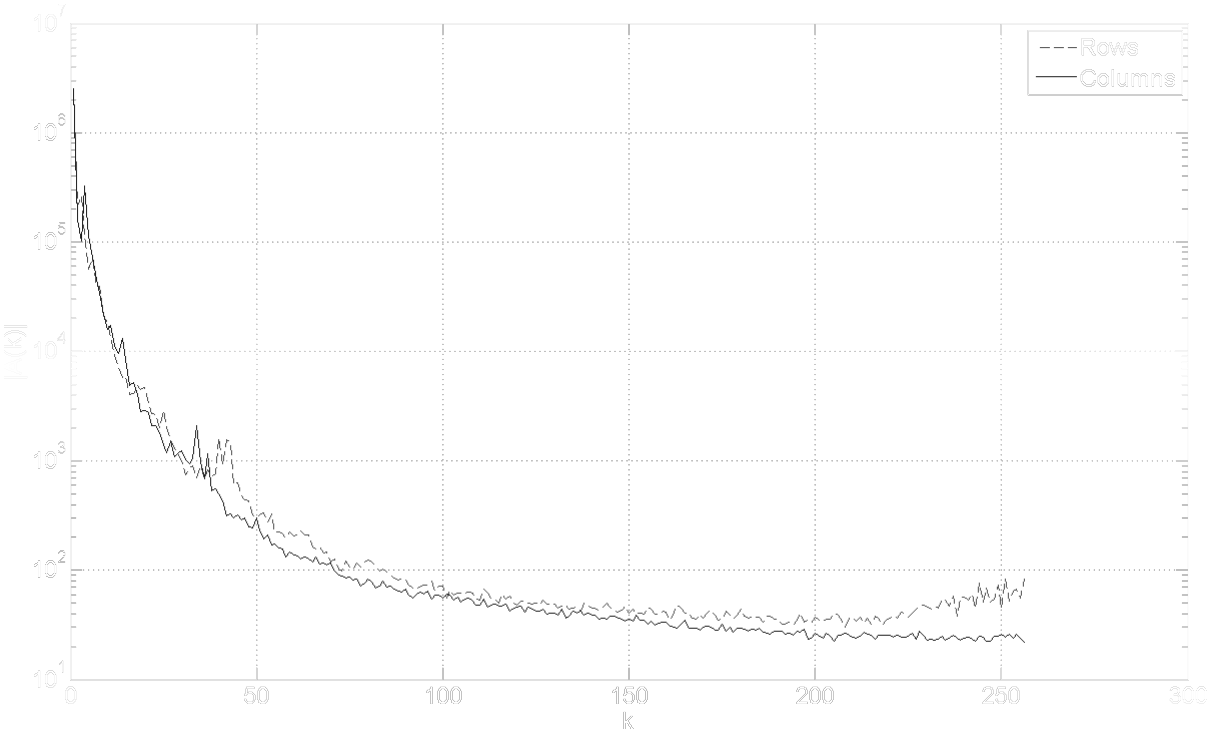

Tab. 1. The investigated sample summary.

Description	**Sample 1**	**Sample 2**	**Sample 3**
Sample material	Gold	Painted coating with defects	CD-ROM
Sample size [μm]	7.03 x 7.03	35.14 x 35.14	2.54 x 2.54
Scan size [pixels]	256 x 256	692 x 692	512 x 512
Scanning direction	Vertical – from top to left	Vertical – from top to left	Vertical – from top to left
Impedance scan			
Scanning speed [μm/s]	8.97	70.84	9.94
Excitation voltage	200 mV at 1 kHz	200 mV at 1 kHz	1 V at 4 kHz
AFM scan			
Scanning speed [μm/s]	8.97	70.84	9.94

Table 1.